Available online at www.sciencedirect.com
SCIENCE DIRECT
Thermochimica Acta 447 (2006) 22–29
thermochimica acta
www.elsevier.com/locate/tca

The role of Rh on a substituted Al Anderson heteropolymolybdate: Thermal and hydrotreating catalytic behavior

Carmen I. Cabello [a,*,1], Mercedes Muñoz [a], Irma L. Botto [b], Edmond Payen [c]

[a] *Centro de Investigación y Desarrollo en Ciencias Aplicadas Dr. Jorge J. Ronco, CINDECA (CONICET-Universidad Nacional de La Plata), Calle 47 N° 257, (1900) La Plata, Buenos Aires, Argentina*
[b] *Centro de Química Inorgánica CEQUINOR (CONICET-Universidad Nacional de La Plata), (1900) La Plata, Buenos Aires, Argentina*
[c] *Unité de Catalyse et de Chimie du Solide, UCCS UMR CNRS 8181, Université des Sciences et Technologies de Lille, Bât. C3, 59655 Villeneuve d'Ascq Cedex, France*

Received 11 January 2006; received in revised form 21 April 2006; accepted 25 April 2006
Available online 4 May 2006

Abstract

The influence of Rh heteroatom on the molybdenum reducibility in the Anderson-type heteropolyoxomolybdate structure of formula $(NH_4)_3[RhMo_6O_{24}H_6]\cdot 7H_2O$ was investigated by means of TPR technique. With comparative purposes, the thermal behavior in non-reducing conditions was also carried out by means of TGA–DTA studies. The study was performed by XRD, SEM, EDAX and FTIR–Raman techniques. Results were related to those preliminary measurements over other XMo_6 Anderson phases. Likewise, Rh(III)–Al(III) formal replacement in the $RhMo_6$ structural arrangement was proved. The formation of a solid solution in a limited range of composition (up to 0.25 Rh) was established in order to explore the catalytic performance of γ-Al_2O_3 supported planar heteropolyoxomolybdate, aiming at optimizing the noble metal content in the catalytic system. Preliminary measurements of $RhMo_6/\gamma$-Al_2O_3 and (Rh, Al)Mo_6/γ-Al_2O_3 activity for HDS and HYD processes were also performed. These results were compared to those obtained for $CoMo_6/\gamma$-Al_2O_3 system in similar operating conditions and other conventional catalytic systems. The potentiality and scope of $RhMo_6$ catalytic system for the HDS and HYD processes were analyzed.

Keywords: Thermal behavior of heteropolyoxomolybdates; Rh and Al Anderson phases; Rh–Mo/γ-Al_2O_3; Rh promoting effect; Hydrotreating catalysts

1. Introduction

Bimetallic systems containing molybdenum and transition metals such as Co, Cr, Ni or Cu have proved to be interesting catalytic materials in a great amount of industrial processes [1]. The addition of noble metals (belonging to VIII B group) enhances the catalytic performance. So, the reducibility of metal components in the mixture is increased by synergetic effect, leading to a better activity and selectivity [2,3]. The preparation of these catalysts is usually based on a support co-impregnation process by using ammonium heptamolybdate (AHM) and metal nitrate solutions, respectively [4].

For the last 10 years, the use of heteropolyoxomolybdates (HPOMs) in catalysis has proved to be an interesting alternative to traditional systems. The advantages are particularly related to the topology, well-defined chemical composition and electronic properties of these polymeric arrays [5–9].

Anderson-type heteropolyoxomolybdates of general formula $[XMo_6O_{24}H_x]^{n-}$ (namely XMo_6), where X is a di-, tri-, penta- or hexavalent metal and $x = 6$ or 0, were characterized by the presence of the X heteroatom in a central octahedral cavity of the crown constituted by six edge-sharing MoO_6 octahedra, showing a D_{3d} planar configuration [10]. Thermal and spectroscopic behavior of different Anderson phases were studied and the catalytic applications of the $CoMo_6$ were analyzed in HDS processes [11–18].

Although the design of catalysts based on noble metals must be carefully considered because of their high cost, the adequate combination with other common metals seems to be a reasonable solution. In this sense, Anderson structure allows a good alternative to obtain a desirable combination. Particularly Rh(III) and Al(III) as heteroatoms in this structure form isomorphous heteropolyanions. In this work, the

* Corresponding author. Fax: +54 2214220288.
E-mail address: ccabello@quimica.unlp.edu.ar (C.I. Cabello).
[1] Member of the research staff of CICPBA.

0040-6031/$ – see front matter © 2006 Elsevier B.V. All rights reserved.
doi:10.1016/j.tca.2006.04.014

thermal behavior of the $(NH_4)_3[Rh(III)Mo_6O_{24}H_6]\cdot 7H_2O$ salt, Anderson-type (identified as $RhMo_6$), was studied in oxidizing and reducing conditions, by means of DTA, TGA and TPR techniques. On the other hand, in order to analyze the promoting effect of Rh content in the planar configuration, the $(NH_4)_3[Rh(III)_xAl(III)_{1-x}Mo_6O_{24}H_6]\cdot 7H_2O$ (or [Rh, Al]Mo_6) solid solution was also prepared. The study was carried out by means of XRD, FTIR and Raman and SEM–EDAX techniques. Thermal investigation results were compared with those reported for other related phases as well as ammonium heptamolybdate whereas preliminary measurements of the catalytic activity for HDS–HYD processes were obtained by $RhMo_6$ and (Rh, Al)Mo_6 supported on γ-Al_2O_3. The comparison with the results for other catalytic systems allowed us to analyze the potentiality and scope of the Rh–Mo based system.

2. Experimental

$RhMo_6$ phase was obtained by reaction in solution from AHM and Rh(III) chloride hydrate in the stoichiometric ratio, according to the method previously described [11–13]. The synthesis of (Rh, Al)Mo_6 solid solutions were obtained by adding $Al(NO_3)_3$ solution to the respective AHM and Rh(III) chloride solutions, according to the desired stoichiometry. Characterization of the samples was checked by XRD using a Philips PW 1714 diffractometer (Cu Kα radiation, Ni filtered), FTIR spectroscopy, SEM–EDAX microscopy and chemical analysis by AAS. Cell parameters were refined by means of the Full Prof 3.0 Program [19].

Vibrational analyses were carried out by means of an FTIR spectrometer Bruker IFSS 66 (KBr pellet technique) and a Raman equipment Spex Ramalog 1403 double monochromator equipped with an SCAMP data processor (excitation line 514.5 nm of an Ar ion laser). Additional measurements were carried out with a Raman LabRAM Infinity microprobe (Jobin Yvon) equipped with a liquid nitrogen detector and a frequency-doubled Nd:YAG laser supplying the excitation line at 532 nm. The power at the sample was below 5 mW.

TGA and DTA measurements were carried out by using a Shimadzu Thermoanalyzer (TGA 50 and DTA 50), heating rate of 10 °C/min and α-Al_2O_3 as reference. The temperature was increased up to 1000 °C. Additional thermal studies were carried out in a furnace, using similar conditions to those of TGA–DTA measurements.

The reduction studies were carried out by using TPR technique in a home-made reactor fed with 10% H_2 reducing agent in N_2 (100 cm^3/min) from 20 to 1000 °C. The heating rate was 5 °C/min. The consumed H_2 was detected by a thermal conductivity cell.

Samples were also investigated by scanning electron microscope Philips SEM 505 with an EDAX 9100 energy dispersive system for X-ray microanalysis. The probe size used was 200 nm.

Supported catalysts were prepared by equilibrium impregnation of γ-Al_2O_3 (226 m^2/g, pore volume of 0.65 cm^3/g and a grain size of 200 μm) with aqueous solutions of $RhMo_6$ or (Rh, Al)Mo_6 ammonium salts at RT for 24 h to obtain the equivalent to a monolayer with 6 wt% Mo and 1 wt% metal, following the procedure given in previous works [14–18]. In addition, the [$RhMo_6$ + $AlMo_6$]/γ-Al_2O_3 combined system was prepared by using a mixed solution of both Rh and Al heteropolyoxomolybdates.

Preliminary measurements of the thiophene hydrodesulfurization and cyclohexene hydrogenation activity were done in a high pressure reactor (at 280 °C, 4 h). The experimental conditions for the activity tests were a feedstock of thiophene (15,000 ppm), cyclohexane (90%) and cyclohexene (10%) flow rate 0.353 ml/min, total pressure 26 kg/cm^2 and LHSV = 52 l/h. Operative conditions for the hydrotreating test were selected according to those used for $CoMo_6$ [15–18].

3. Results and discussion

3.1. Synthesis and characterization of Anderson phases involving Rh

The $RhMo_6$ phase was identified by XRD and SEM microscopy. The chemical analysis data on the basis of Rh and Mo contents of the Anderson stoichiometry by AAS yielded Rh 15.91% and Mo 84.08%, in agreement with the theoretical values (15.16% Rh and 84.83% Mo, respectively).

The replacement of Rh by Al was analyzed for catalytic purposes in order to decrease the Rh content in a structural arrangement. So, the synthesis of [$Rh_{0.25}Al_{0.75}$], [$Rh_{0.5}Al_{0.5}$] and [$Rh_{0.75}Al_{0.25}$] solid solutions was performed. The [$Rh_{0.25}Al_{0.75}$] XRD pattern was similar to that of $RhMo_6$, with the expected slight shift of the diffraction lines upward 2θ angles (lower cell parameters) as it is observed in Fig. 1. However, the lower resolution of the [$Rh_{0.5}Al_{0.5}$]Mo_6 and [$Rh_{0.75}Al_{0.25}$]Mo_6 XRD patterns did not permit to clearly identify the formation of a solid solution with these stoichiometries. Likewise, SEM microscopy revealed similar nanocrystal morphologies in all cases. The [$Rh_{0.25}Al_{0.75}$]Mo_6 and $RhMo_6$ micrographs and EDAX profiles are shown in Fig. 2. EDAX data were in acceptable agreement with the theoretical Rh/Mo ratios for all stoichiometries but

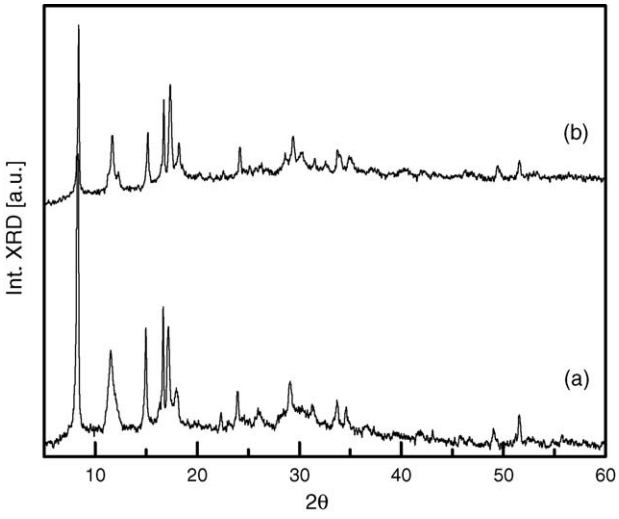

Fig. 1. XRD diagrams of (a) $RhMo_6$ and (b) [$Rh_{0.25}AL_{0.75}$]Mo_6 ammonium salts.

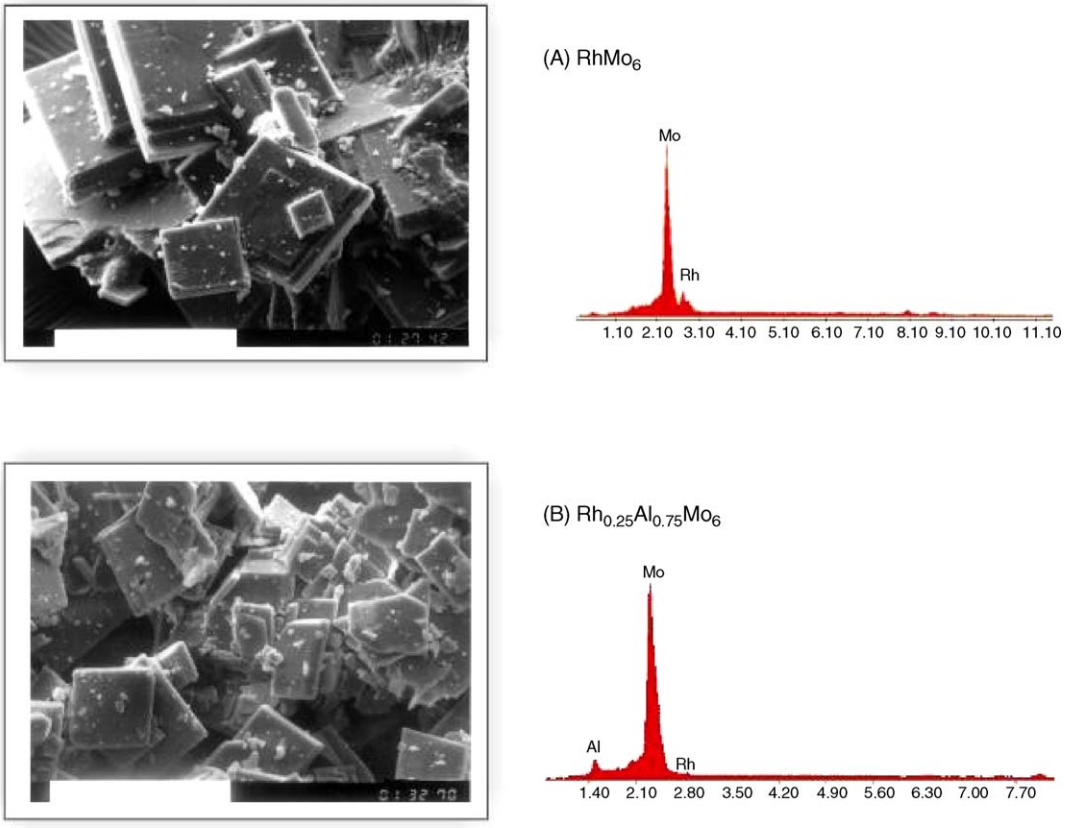

Fig. 2. SEM micrograph and EDAX signals of: (A) $RhMo_6$ (magnification: ×500, scale bar: 100 μm) and (B) $[Rh_{0.25}AL_{0.75}]Mo_6$ (magnification: ×500, scale bar: 100 μm).

the Rh distribution for $[Rh_{0.5}]$ and $[Rh_{0.75}]$ was not uniform, evidencing the co-existence of both $AlMo_6$ and $RhMo_6$ end members of the solid solution separately. Thus, the formation of a solid solution was only possible in a limited range of composition due to the great difference between the trivalent ionic radii ($r_{Al(III)} = 0.535$ Å and $r_{Rh(III)} = 0.665$ Å, respectively).

It is well known that HPOMs are predominantly characterized by the presence of Mo–O bridged and $Mo–O_{2t}$ terminal bonds, which can be considered as "closed" moieties [10,12]. Such bonds directed outwards seem to be the most sensible to heteroatom exchange. So, vibrational spectroscopy can provide valuable information about this effect [11,12]. The $[Rh_{0.25}Al_{0.75}]Mo_6$ FTIR spectrum (not shown here) is typical of Anderson structure, with $Mo–O_{2t}$ terminal bonds located at 940 cm^{-1} (ν_s) and 889 and 852 cm^{-1} (ν_{as}), $Mo–O_b$ and $Mo–O_c$ bridge bonds at 636 and 341 cm^{-1}, the Rh–O stretching at 575 cm^{-1} and water librations at 429 cm^{-1} [11,12]. However, the sharp lines of Raman spectroscopy, unlike the FTIR high band-widths of the primary Mo-O units, which did not permit to reveal accurately the Al–Rh substitution, are useful to analyze the problem [11,12]. Fig. 3 shows Raman spectra of $[Rh_xAl_{1-x}]Mo_6$ (with $x = 1$, 0.25 and 0) and Table 1 compares the main Mo–O Raman modes for the $RhMo_6$, $AlMo_6$ and real and hypothetical intermediate members of the solid solution. The highest nuclear charge of Rh(III) is responsible for the reinforcement of both Mo–O terminal bonds and $Mo–O_b$ ones by inductive effect [11–16]. Hypothetical $[Rh_xAl_{1-x}]Mo_6$ [$x = 0.75$ and 0.5] solid solution showed lines located at 947, 901 and near 565 cm^{-1} like the $[Rh_{0.25}Al_{0.75}]Mo_6$ phase. The most sensitive band corresponds to Mo–Ob stretching which is useful to reveal the limit of the solid solution corroborating the previously suggested inhibition to form a continuous solid solution between $RhMo_6$ and $AlMo_6$. The discontinuity, attributed to the noticeable difference between the heteroatom ionic radii (∼20%), led

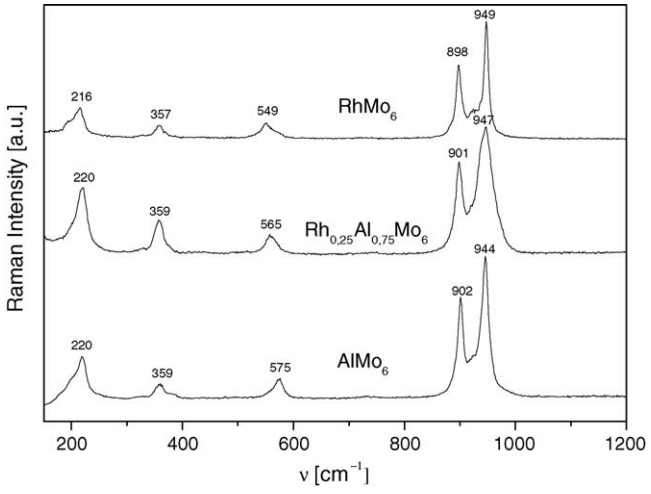

Fig. 3. Raman spectra of XMo_6 ammonium salts (between 1200 and 150 cm^{-1}).

Table 1
Raman data of $RhMo_6$, $AlMo_6$ and $[Rh_xAl_{(1-x)}]Mo_6$ (between 1200 and 550 cm^{-1})

Phase	ν_s Mo–O_{2t} (cm^{-1})	ν_{as} Mo–O_{2t} (cm^{-1})	ν Mo–O_b (cm^{-1})
$RhMo_6$	949	898	549
$[Rh_xAl_{(1-x)}]Mo_6$[a]	947	901	565–569
$[Rh_{0.25}Al_{0.75}]Mo_6$	947	901	565
$AlMo_6$	944	902	575

[a] Hypothetical phase with $x = 0.5$ and 0.75.

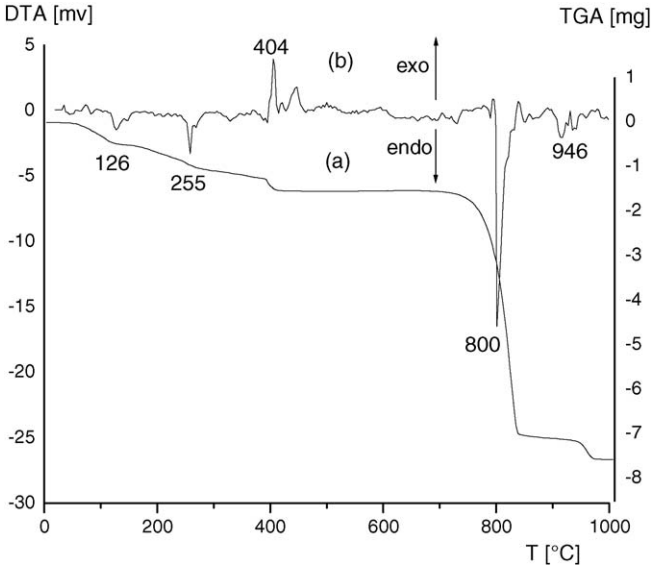

Fig. 4. (a) TGA and (b) DTA curves of $RhMo_6$.

to the formation of Al-rich members (up to $x \sim 0.25$) and thus only $[Rh_{0.25}Al_{0.75}]Mo_6$ HPOMs will be considered hereafter.

3.2. Thermal treatment of $RhMo_6$ in oxidizing atmosphere

TGA–DTA curves, recorded between RT and 1000 °C, are shown in Fig. 4(a and b) and the results are summarized in Table 2. Thermal analysis up to 450 °C showed the typical behavior of the Anderson phases with three mass-losses at 126, 255 and 404 °C, respectively [12,13]. The first one is reversible and attributed to the dehydration process. The resolution of the second one, assigned to the release of NH_3 and H_2O (from the countercation and partially from intermolecular H) was not well defined, whereas the third mass-loss, associated to the collapse of the anionic structure with the removal of the remaining water molecules, occurred at ∼420 °C. Although the product obtained at this temperature was amorphous to XRD, further heating allowed to reveal the Rh_2MoO_6 rutile-type phase which was clearly detected by XRD at 600 °C (plus MoO_3 diffraction lines). The $RhMo_6$ thermal behavior showed differences from that observed for $CoMo_6$, $AlMo_6$ and $CuMo_6$ [13,20]. Whereas the first one stabilized the Co(II) species such as Co(II)MoO_4, the second one formed $Al_2(MoO_4)_3$ and the last yielded CuO as temperature increased. For the $RhMo_6$ phase, the evolution of MoO_3 from ∼750 °C, according to TGA curve, led to Rh_2MoO_6 like the unique oxide phase, which remained stable up to ∼950 °C. The calculated cell parameters deduced from XRD data by using a tetragonal cell ($a = 4.61$ Å and $c = 3.03$) are in agreement with those given in PDF pattern 30–0848. The Mo–Rh rutile-type oxide decomposed at ∼950 °C into MoO_3 and Rh_2O_3, respectively. SEM micrographs and EDAX profiles shown in Fig. 5 correspond to samples thermally treated and enable us to observe the morphological and chemical data changes during the $RhMo_6 \rightarrow Rh_2MoO_6 + MoO_3 \rightarrow Rh_2O_3$ sequence.

Comparative EDAX data also contributed to analyze the oxidative thermal effect. The original Rh/Mo ratio (0.18) increased to 2.20 by heating at 850 °C (68.77% Rh, 31.23% Mo) in agreement with Rh_2MoO_6 theoretical value of 2.15 (Rh = 68.20%, Mo = 31.80%).

Regarding the formation of the trirutile phase, it should be pointed out that Rh and Mo octahedral environment in the original Anderson-type heteropolyoxoanion should be structurally displaced and re-arranged to form MoO_3 and the mixed oxide, both with the metals in octahedral coordination. The variability of EDAX results at 750 °C (from 36.43% Rh and 63.57% Mo to 100% Mo) can be attributed to the intermediate step to obtain the mixed oxide and the MoO_3 segregation. The different thermal stability of both oxides enabled to establish the existence of the mixed oxide, as unique phase, in the temperature range between ∼800 and ∼950 °C.

3.3. Thermal treatment in reducing atmosphere

Fig. 6(a) shows the TPR pattern of $RhMo_6$ phase. This is characterized by an intense signal at 285 °C. Several signals of lower intensity are observed in the 390–500 °C region as well as at 732 °C. The pattern was appreciably different from those corresponding to the $CoMo_6$ studied phase (with signals at 610 and 848 °C) and from $AlMo_6$ identified in the figure as pattern (c). The mentioned phases as well as ammonium heptamolybdate present two sharp signals, basically attributed to Mo(VI)–Mo(IV) and Mo(IV)–Mo° reduction steps which are observed in the ranges of 580–730 and 850–990 °C, respec-

Table 2
TGA–DTA data of $(NH_4)_3[RhMo_6O_{24}H_6]\cdot 7H_2O$ ($RhMo_6$)

T (°C) (exo ⇑, endo ⇓)	TGA data mass-loss (wt%)	Process	Theoretical mass-loss (wt%)	Solid residue (according to XRD)
126	9.60	Dehydration	10	Amorphous
255	13.65	$-H_2O$, $-NH_3$	14.42	Amorphous
404	18.48	$-H_2O$, $-NH_3$	18.87	Amorphous, Rh_2MoO_6 and MoO_3 from 600 °C
800	83.88	$-MoO_3$	84.07	Rh_2MoO_6
946	89.58	$-MoO_3$	89.83	Rh_2O_3

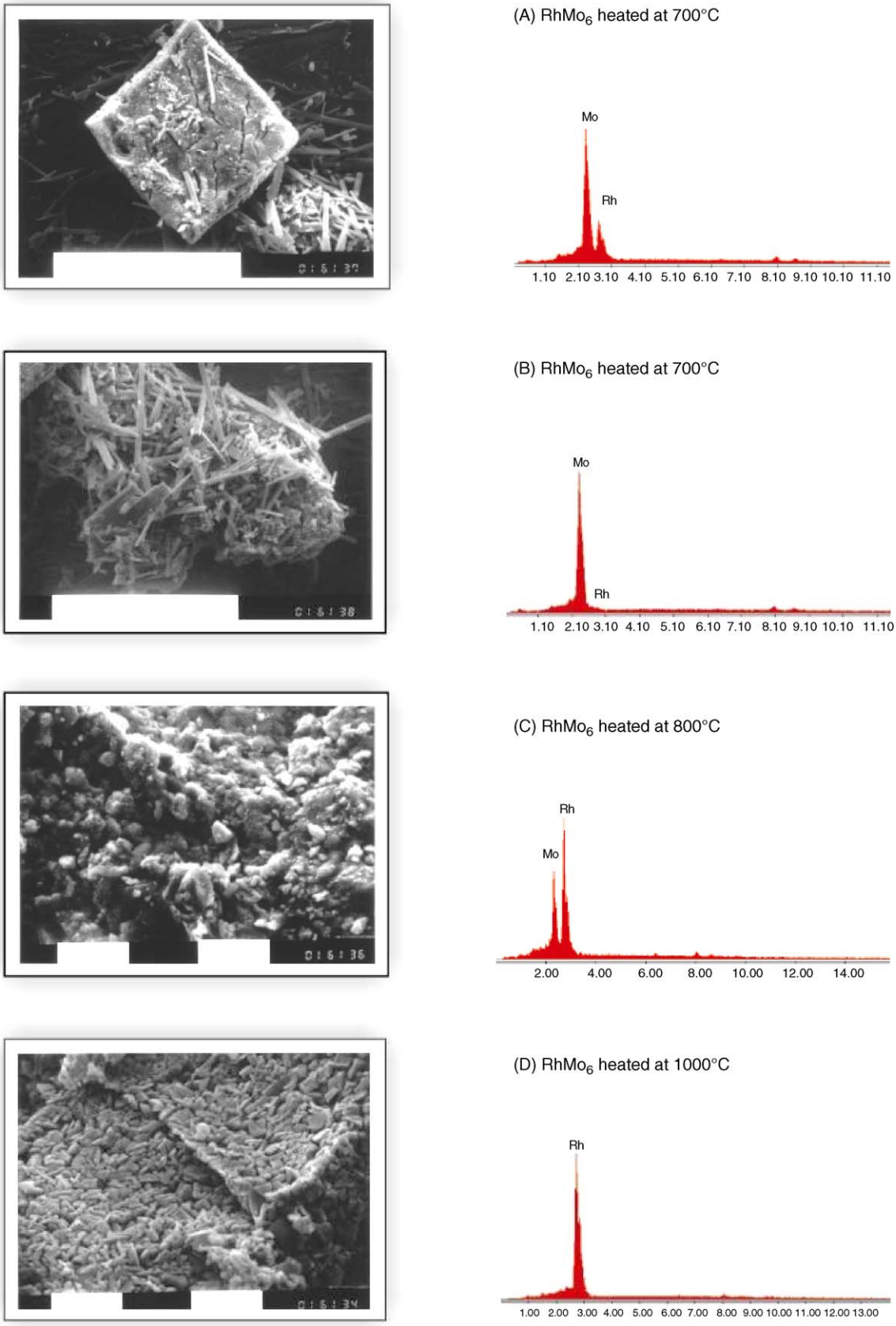

Fig. 5. SEM micrographs and EDAX signals of $RhMo_6$ samples corresponding to several stages of thermal treatment (in air atmosphere). Sample heated at: (A) (magnification: × 680, scale bar = 100 μm) and (B) magnification: × 650, scale bar = 100 μm), 700 ° C; (C) (magnification: × 2500, scale bar = 10 μm) 800 °C and (D) magnification: × 2500, scale bar = 10 μm) 1000 °C.

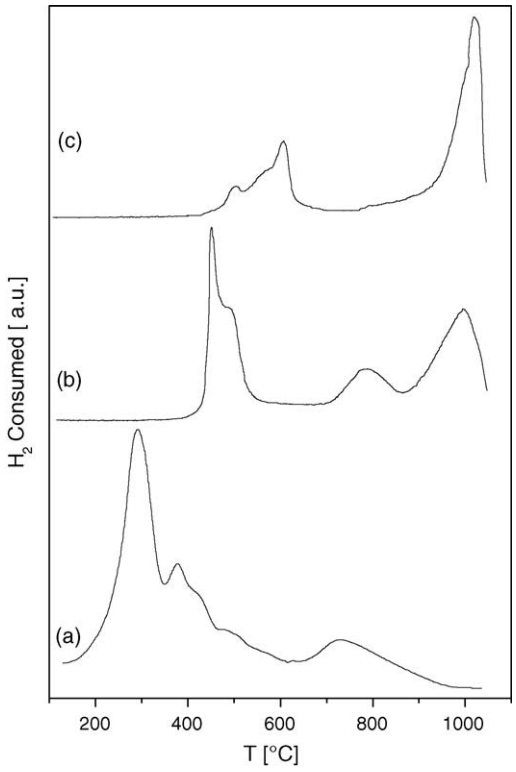

Fig. 6. TPR patterns of: (a) $RhMo_6$, (b) $[Rh_{0.25}Al_{0.75}]Mo_6$ and (c) $AlMo_6$.

tively (although the low temperature signal can also include the heteroatom reduction, as in the $CoMo_6$ phase) [13,20]. Pattern (b) corresponds to $[Rh_{0.25}Al_{0.75}]Mo_6$ solid solution, which partially resembles $RhMo_6$ and $AlMo_6$ as well. In this case, the strongest signal is shifted to higher temperatures (∼500 °C). On the other hand, the Rh(III)–Rh° reduction in Rh_2O_3 oxide occurs at 135 °C [21], temperature which is lower than that observed for the $RhMo_6$ phase (286 °C). This effect can be related to a higher metal stability in the condensed structure. TPR data of $RhMo_6$, $AlMo_6$ and $CoMo_6$ Anderson phases are given in Table 3 where AHM values are also included for comparative purposes. The products of the reduction by XRD are also given.

Samples of $RhMo_6$ after TPR at 400 °C were amorphous to XRD and the presence of MoO_2 can be suggested from ∼650 °C by the very weak X-ray signals corresponding to the most intense peaks of the monoclinic MoO_2 oxide (PDF 86–0135). XRD features of Rh and Mo metals were weak at this temperature, suggesting a high degree of metallic dispersion (PDF of Rh 87–0714, PDF of Mo 42–1120).

EDAX data of TPR samples showed an increase of Mo content (89%) at 400 °C and a subsequent decrease (85%) at 1000 °C. This effect can be associated to the reduction progress of Mo(VI)–Mo(IV) and partially to Mo(IV)–Mo° processes, both included in a stronger low temperature signal. Therefore, the outer skin of the system was enriched by molybdenum [13]. The complete reduction of remaining MoO_2 was observed at 732 °C, yielding a Mo/Rh ratio similar to that of the original sample.

The high reducibility of $RhMo_6$ phase can be related to the oxidizing character of the heteroatom ($E^{\circ}_{Rh(III)-Rh^{\circ}} = 0.44$ V) which affects the stability of Mo(VI). The $AlMo_6$ pattern, useful as reference, clearly presents a double area for Mo(IV)–Mo° (second stage at ∼990 °C) in relation to Mo(VI)–Mo(IV) (first stage at 586 °C). The area of $RhMo_6$ TPR second signal was very weak with respect to the first one, thus showing the Rh° promoting effect. Therefore, the higher heteroatom reducibility, the higher molybdenum reducibility and the lower reduction temperature. The characteristics of this type of reduction (high rate and low temperature) inhibit the adequate atomic arrangement affecting not only the size and dispersion of the metal particles, but also the nucleation and growth of the oxidic intermediate product. Consequently, the MoO_2 crystallinity is very poor. Typical XRD patterns of Mo and Rh were observed after further heating (from ∼1000 °C).

From Fig. 6, it is also interesting to point out the intermediate feature of the $[Rh_{0.25}Al_{0.75}]Mo_6$ TPR pattern which corroborates the existence of a solid solution. Hence, the temperatures and areas of TPR peaks are appreciably changed among end and intermediate members of the solid solution. In fact, the Mo(VI)–Mo(IV) signal for $AlMo_6$ phase occurs at about ∼300 °C above that of $RhMo_6$. Besides, the weak peak at 732°C for $RhMo_6$ differs significantly from the strongest signal at ∼1000 °C for the $AlMo_6$ phase. Regarding the solid solution, the formation of Mo° in the first step is associated to the Rh content in the structure. Likewise, the shift of the TPR signal from 285 °C (for $RhMo_6$) up to 586 °C (for $AlMo_6$) is in agreement with the decrease of Rh amount. The correlation between

Table 3
Comparison among the TPR results of different Anderson phases and ammonium heptamolybdate (AHM) (Effects of heteroatom reducibility on the molybdenum reduction)

Phase	Heteroatom reduction potential (V)	Temperature of Mo(VI)–Mo(IV) process (°C)	Products	Temperature of Mo(IV)–Mo process (°C)	Products
$RhMo_6$	0.44	285	Rh, MoO_2, Mo	732	Rh, Mo
$CuMo_6$	0.34	374–385	Cu, MoO_2	783	Cu, Mo
$CoMo_6$	1.80[a], −0.28[b]	610	$CoMoO_4$, MoO_2	848	Co, Mo
$AlMo_6$	−1.66	586	MoO_2[c]	990	Mo, Al_2O_3
AHM		730	MoO_2	850	Mo

[a] Co(III)–Co(II).
[b] Co(II)–Co.
[c] "(Mo, Al)O_2" reduced non-stoichiometric rutile-type phase [13].

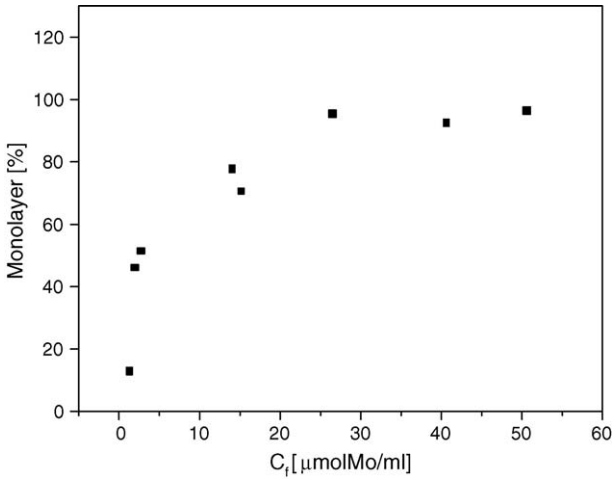

Fig. 7. $RhMo_6$ adsorption isotherm on γ-Al_2O_3.

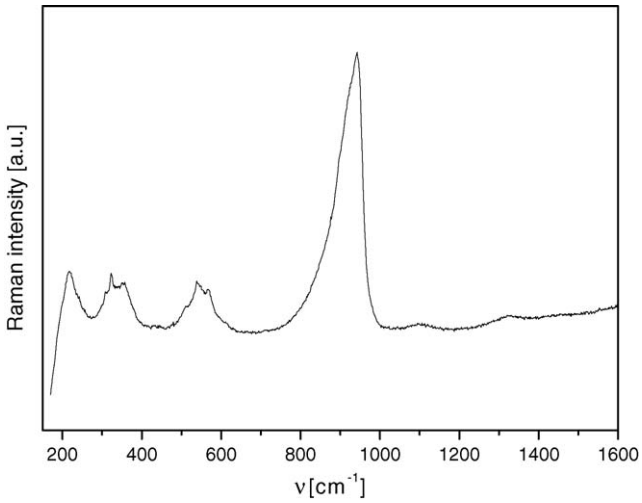

Fig. 8. Raman spectrum of γ-Al_2O_3 supported $RhMo_6$.

the reducibility of the system and the proportion of Rh to promote the hydrogen spillover allows us to design the appropriate combination in a suitable structure to ensure the reducibility of molybdenum at a given temperature.

3.4. Preliminary data of catalytic activity

The potentiality of $RhMo_6$ phase in catalysis was analyzed by means of the results of the above-mentioned thermal behavior. Preliminary data of thiophene hydrodesulfurization (HDS) and cyclohexene hydrogenation (HYD) activities for the catalysts based on $RhMo_6$ and [Rh, Al]Mo_6 supported on γ-Al_2O_3 are reported. They were prepared by equilibrium adsorption of the support given in the experimental item, following the operative conditions given in previous works [14–18]. AAS chemical analysis and the isotherm adsorption curve (shown in Fig. 7) for the $RhMo_6/\gamma$-Al_2O_3 system revealed a monolayer of 6% Mo and 1% Rh (g metal/100 g γ-Al_2O_3). The corresponding data for $[Rh_{0.25}, Al_{0.75}]Mo_6$ solid solution were 5% Mo and 0.23% Rh [14].

The $RhMo_6$ phase supported on γ-Al_2O_3 was characterized by Raman spectroscopy. Fig. 8 shows the Raman spectrum, which exhibits the main line characteristic of the MoO_{2t} stretching mode at 947 cm^{-1}. However, the comparison between supported and unsupported $RhMo_6$ phase showed a broadening of this Raman line, revealing some structural modifications of the $RhMo_6$ starting material as previously observed for the other Anderson phases [16]. Indeed, during the impregnation stage, it is known that electrostatic ion–support interactions, coordinative ion–surface bonding, Al(III) dissolution with formation of $AlMo_6$; Rh(III) diffusion reactions on the support surface, etc., may intervene [14,22–24]. So, in this case, the support dissolution, the subsequent $AlMo_6$ phase formation, its re-precipitation on the support as well as the Rh(III) diffusion to form [Rh, Al]Mo_6 solid solution could be suggested.

Table 4 shows chemical data and catalytic conversion of some of $RhMo_6$ based catalysts. Data of $CoMo_6/\gamma$-Al_2O_3, CoMo commercial [14–18], Rh commercial catalysts and a TPR treated $RhMo_6/\gamma$-Al_2O_3 at 200 °C catalysts are included for comparative purposes. This table clearly shows the role that Rh plays in the enhancement of the Mo catalytic system. Whereas the reducibility of Rh increases the hydrogenation ability, the catalytic performances in HDS are similar to those observed in the $CoMo_6$ supported system. The synergetic effect observed in the heteropolyanion array with a low Rh/Mo ratio seems to be promising.

However, the decrease of Rh content, observed in the solid solution, affects HYD as well as HDS activities [2].

Table 4
Chemical data and conversion of thiophene and cyclohexene for different $RhMo_6$ catalytic and reference systems

γ-Al_2O_3 supported catalysts	X [%]	Mo [%]	HYD [%]	S_{HYD}	HDS [%]	S_{HDS}
$CoMo_6$	0.80	8.00	30.00	37.50	70.81	8.85
CoMo[a]	1.80	9.30	15.55	8.63	71.00	7.63
$RhMo_6$	1.00	6.00	84.68	84.68	72.40	12.06
$[Rh_{0.25}Al_{0.75}]Mo_6$	0.23	5.00	10.00	43.50	21.00	4.20
[$RhMo_6$ + $AlMo_6$][b]	0.50	6.00	55.00	100.00	50.14	8.35
$RhMo_6$[c]	1.12	6.80	66.80	59.64	13.70	2.01
Rh[a]	5.00	–	65.00	13.00	22.38	–

Note: X [%] and Mo [%] are total metal concentration in g/100 g support. S_{HYD} and S_{HDS} = HYD/X [%] (Co or Rh) and HDS/Mo [%].

[a] Commercial catalysts.

[b] Catalyst prepared by $RhMo_6/AlMo_6$ combined solutions.

[c] Catalyst after TPR condition treatment at 200 °C.

Both catalysts [solid solution [$Rh_{0.25}$, $Al_{0.75}$]Mo_6 and [$RhMo_6$ + $AlMo_6$]/γ-Al_2O_3 combined system (0.5$RhMo_6$/0.5$AlMo_6$)] reveal a catalytic effect depending on Rh content.

The reducing thermal pre-treatment of $RhMo_6$/γ-Al_2O_3 induced a substantial decrease of HDS activity whereas HYD activity was not so affected. The presence of Rh induced the Mo(VI)–Mo(IV) reduction at lower temperature.

These Mo(IV) species were then poorly sulfided upon activation, which affected the catalytic performance as it is widely described in literature [25,26].

4. Conclusions

The main results of this work dealing with $RhMo_6$ system can be summarized as follows:

(i) Upon thermal treatment in oxidative conditions of bulk $RhMo_6$, the formation of the trirutile $RhMo_2O_6$ phase, stable in the range between 700 and 950 °C is observed, whereas in reducing conditions Rh acts as promoter of the Mo reduction. The reduction behavior is different from the one observed for the other Anderson phases. Indeed, the presence of Rh metal induces the complete Mo(VI)–Mo(IV)–Mo° reduction at low temperatures (from ∼250 °C). However, the Rh(III) reducibility to form Rh° occurs at higher temperature than that observed in Rh–O binary systems due to the stability of the heteropolyanion structure.

(ii) The formation of a bulk solid solution between $RhMo_6$ and $AlMo_6$ phases is not complete and it is observed in a small range of Rh content (up to 0.25 M ratio or [$Rh_{0.25}$,$Al_{0.75}$]Mo_6). This fact can be attributed to the differences between the trivalent ionic radii of the heteroatoms.

(iii) HDS activity of $RhMo_6$/γ-Al_2O_3 catalyst is similar to that observed for $CoMo_6$/γ-Al_2O_3 and Co–Mo/γ-Al_2O_3 systems. Likewise, its HYD activity is considerably higher than that for the commercial Rh/γ-Al_2O_3 catalyst.

Catalytic performance of this bifunctional system is a promising target to be explored more accurately.

Acknowledgements

This work was supported by CONICET; CICPBA Argentina and COCAFAL Program (CNRS France and TOTAL). We are grateful to Mrs. Pascale Baranek, Mrs. Graciela Valle, Lic. Diego Peña and to Lic. Norberto Firpo for their contribution in experimental measurements. C.I. Cabello is a member of the research staff of CICPBA, Argentina.

References

[1] G. Ertl, H. Knozinger, J. Weitkamp (Eds.), Handbook of Heterogeneous Catalysis, vol. 1, VHC, Weinheim, 1997, p. 278.
[2] Z. Vít, D. Gulková, L. Kaluza, M. Zdrazil, J. Catal. 232 (2005) 447.
[3] C. Bianchi, Catal. Lett. 76 (2001) 155.
[4] M. Shelef, G.W. Graham, Catal. Rev. Sci. Eng. 36 (6) (1994) 433.
[5] C. Cáceres, M.N. Blanco, H.J. Thomas, in: G. Poncelet, P. Grange, P.A. Jacobs (Eds.), Preparation of Catalysts III, Elsevier, Amsterdam, 1983, p. 333.
[6] M.T. Pope, A. Müller (Eds.), Polyoxometalate chemistry from topology via self-assembly to applications, Kluwer Academic Publishers, London, 2001.
[7] M. Misono, Catal. Rev. Sci. Eng. 29 (1987) 269.
[8] N. Mizuno, M. Misono, Chem. Rev. 98 (1) (1998) 199.
[9] D. He, D. Pang, L. Wei, Y. Chen, T. Wang, Z. Tang, J. Liu, Y. Liu, Q. Zhu, Catal. Commun. 3 (2002) 429.
[10] M.T. Pope, Heteropoly and Isopolyoxometallates, Springer-Verlag, Berlin, 1983.
[11] I.L. Botto, A.C. Garcia, H.J. Thomas, J. Phys. Chem. Solids 53 (8) (1992) 1075.
[12] C. Martin, C. Lamonier, M. Fournier, O. Mentré, V. Harlé, D. Guillaume, E. Payen, Inorg. Chem. 43 (2004) 4636.
[13] C.I. Cabello, I.L. Botto, H.J. Thomas, Thermochim. Acta 232 (1994) 183.
[14] C.I. Cabello, I.L. Botto, F. Cabrerizo, M.G. González, H.J. Thomas, Ads. Sci. Tech. 18 (7) (2000) 591.
[15] C.I. Cabello, I.L. Botto, H.J. Thomas, Appl. Catal. A 197 (2000) 79.
[16] I. Pettiti, I.L. Botto, C.I. Cabello, S. Colonna, M. Faticanti, G. Minelli, P. Porta, H.J. Thomas, Appl. Catal., A: Gen. 220 (1–2) (2001) 113.
[17] C.I. Cabello, F.M. Cabrerizo, A. Alvarez, H.J. Thomas, J. Mol. Catal. A Chem. 186 (2002) 89.
[18] C.I. Cabello, M. Muñoz, E. Payen, H.J. Thomas, Catal. Lett. 92 (2004) 69.
[19] J. Rodriguez-Carvajal, Phys. B 192 (1993) 55.
[20] I.L. Botto, C.I. Cabello, G. Minelli, M. Occhiuzzi, Mater. Chem. Phys. 39 (1994) 21.
[21] A. Jones, B. Mc Nicol, Temperature Programmed Reduction for Solid Materials Characterization, Marcel Dekker, New York, 1986, p. 109.
[22] I.L. Le Bihan, P. Blanchard, M. Fournier, J. Grimblot, E. Payen, J. Chem. Soc., Faraday Trans. 94 (1998) 937.
[23] X. Carrier, J.F. Lambert, M. Che, J. Am. Chem. Soc. 119 (1997) 10137.
[24] X. Carrier, J.B. D'Espinose de la Caillerie, J.F. Lambert, M. Che, J. Am. Chem. Soc. 121 (1999) 3377.
[25] D. Pirotte, J.M. Zabala, P. Grange, B. Delmon, Bull. Soc. Chim. Belg. 90 (1981) 1239.
[26] H. Topsøe, B.S. Clausen, F.E. Massoth, in: J.R. Anderson, M. Boudart (Eds.), Catalysis Science and Technology, vol. 11, Springer-Verlag, Berlin, 1996.